MeV-level electron and gamma ray sensitivites of modern far ultraviolet sensitive microchannel plate detectors

MeV-level electron and gamma ray sensitivites of modern far ultraviolet sensitive microchannel plate detectors

Michael W. Davis, Thomas K. Greathouse, Chathan M. Cooke, Ryan C. Blase, G. Randall Gladstone, et al.

Michael W. Davis, Thomas K. Greathouse, Chathan M. Cooke, Ryan C. Blase, G. Randall Gladstone, Kurt D. Retherford, "MeV-level electron and gamma ray sensitivites of modern far ultraviolet sensitive microchannel plate detectors," Proc. SPIE 9915, High Energy, Optical, and Infrared Detectors for Astronomy VII, 99152B (27 July 2016); doi: 10.1117/12.2232755

SPIE.

Event: SPIE Astronomical Telescopes + Instrumentation, 2016, Edinburgh, United Kingdom

MeV-level electron and gamma ray sensitivities of modern far ultraviolet sensitive microchannel plate detectors

Michael W. Davis*[a], Thomas K. Greathouse[a], Chathan M. Cooke[b], Ryan C. Blase[a], G. Randall Gladstone[a], Kurt D. Retherford[a]

[a] Southwest Research Institute, 6220 Culebra Road, San Antonio, TX, USA 78238-5166; [b]Research Laboratory of Electronics, Massachusetts Institute of Technology, Cambridge, MA 02139

ABSTRACT

The Jovian system is the focus of multiple current and future NASA and ESA missions, but dangerously high radiation levels surrounding the planet make operations of instruments sensitive to high energy electrons or gamma rays problematic. Microchannel plate (MCP) detectors have been the detectors of choice in planetary ultraviolet spectrographs for decades. However, the same properties that give these detectors high response to vacuum ultraviolet photons also make them sensitive to high energy electrons and gamma rays. The success of ultraviolet investigations in the Jovian system depends on effectively shielding these MCP detectors to protect them as much as possible from this withering radiation. The design of such shielding hinges on our understanding of the response of MCP detectors to the high energy electrons and gamma rays found there. To this end, Southwest Research Institute and Massachusetts Institute of Technology collaborated in 2012-13 to measure the response of a flight-spare microchannel plate detector to a beam of high energy electrons. The detector response was measured at multiple beam energies ranging from 0.5-2.5 MeV and multiple currents. This response was then checked with MCNP6, a radiation transport simulation tool, to determine the secondary gamma rays produced by the primary electrons striking the detector window. We report on the measurement approach and the inferred electron and gamma sensitivities.

Keywords: ultraviolet detectors, microchannel plate detectors, radiation effects, high energy electrons, gamma rays, Jupiter

1. INTRODUCTION

Southwest Research Institute (SwRI) has been a leader in the development and flight of compact ultraviolet imaging spectrographs for planetary missions for over twenty years. Rosetta-Alice, the first of four spectrographs now in-flight, was developed for the Rosetta mission and has orbited comet Churyumov-Gerasimenko since August 2014[1]. New Horizons's Pluto-Alice, the second, was developed for the New Horizons mission and flew past Jupiter in February 2007 and Pluto in July 2015[2]. The Lyman Alpha Mapping Project (LAMP) was developed for the Lunar Reconnaissance Orbiter (LRO) and has continuously mapped the Moon since August 2009[3]. Finally, the ultraviolet spectrograph for the Juno mission (Juno-UVS) is in flight now and will reach Jovian orbit in July 2016[4]. Two more ultraviolet spectrographs are in development for ESA's JUICE mission to the Jupiter system and NASA's Europa mission. Both missions are currently slated to launch in 2022.

Microchannel plate detectors, the heart of SwRI's ultraviolet spectrographs, are susceptible to the MeV-level electrons found in the Jovian environment. Pluto-Alice detected these electrons during its flyby of the Jovian system in 2007, despite coming no closer than 32 Jupiter radii to the planet[5]. Juno-UVS, JUICE-UVS, and Europa-UVS will all operate much closer to Jupiter than Pluto-Alice did, so they have been designed and/or flown with tantalum shielding to reduce their effective electron dose. However, even with this shielding in place, the detector is expected to see up to ~ 200,000 counts/s backgrounds. Since optimizing instrument shielding mass is always a concern for planetary spacecraft, the authors decided to undergo a study to pin down the expected efficiency of flight-like microchannel plate detectors to MeV-level electrons and the secondary gammas produced when electrons pass through shielding. To this end, the team made two visits to MIT's High Voltage Research Laboratory in July 2012 and November 2013. The first set of tests was compromised by fluorescence of the detector window, so the results of the second set of tests are presented here.

*mdavis@swri.edu; phone 1 210 522-6036; fax 1 210 543-0052

High Energy, Optical, and Infrared Detectors for Astronomy VII, edited by Andrew D. Holland, James Beletic, Proc. of SPIE Vol. 9915, 99152B · © 2016 SPIE · CCC code: 0277-786X/16/$18 · doi: 10.1117/12.2232755

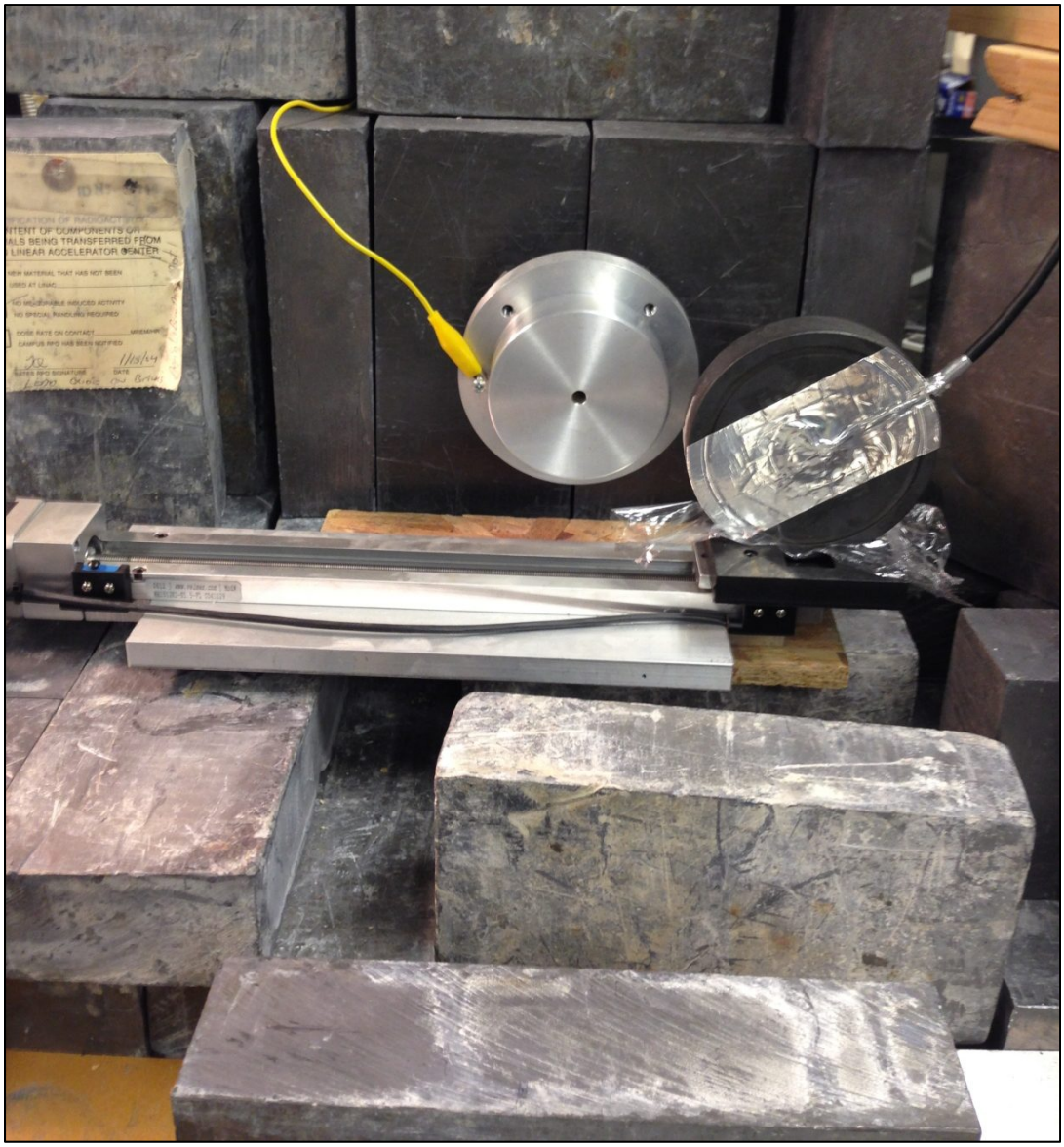

Figure 1. The electron aperture and Faraday Cup at MIT's High Voltage Research Laboratory.

2. EXPERIMENTAL SETUP

The detector efficiency tests were undertaken at MIT's High Voltage Research Laboratory. This facility has the ability to produce monoenergetic electron beams ranging in energy up to 3 MeV for "short" durations (on the order of minutes before stability is lost) or up to 2.5 MeV for longer durations. The beam currents can go as low as 100±50 fA for beams with moderately stable current, or as low as 1.0±0.1 pA for beams with highly stable current. The electrons are generated by a Van de Graaff generator on the facility's ground floor, and then routed via a magnet to an output aperture in a shielded basement. The output "window" is a thin (0.003-inch thick) sheet of aluminum that maintains vacuum in the generator while minimizing secondary Bremsstrahlung generation. The electron energy is measured in vacuum, while the beam current is measured in atmosphere by a Faraday cup on a linear stage that can move in-and-out of the beam during operation. The output and Faraday cup are shown in Figure 1.

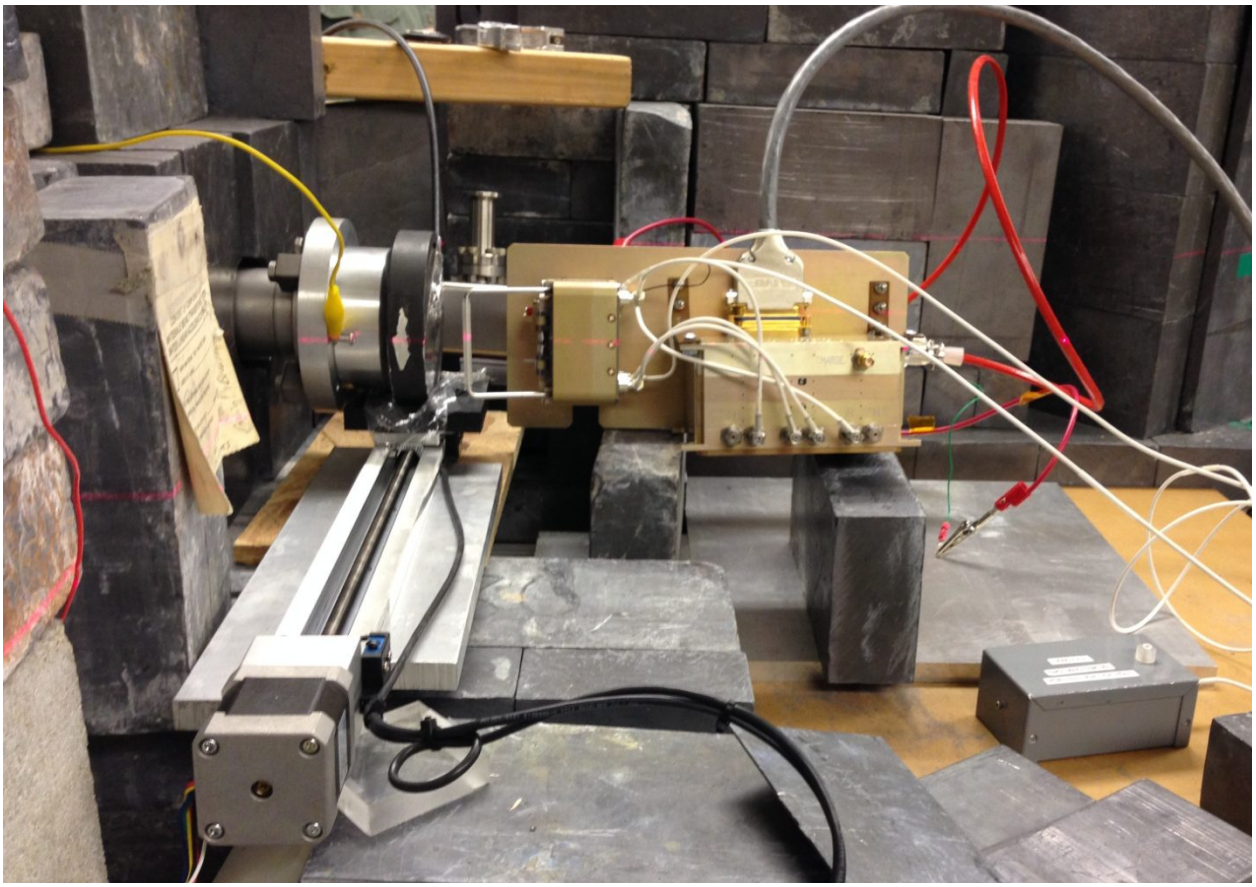

Figure 2. The Juno-UVS flight spare detector and electronics in line with the electron aperture and Faraday cup. Note the laser level line (red) used to ensure alignment of the detector and electron aperture.

The unit under test was the flight spare detector and electronics assembly from the Juno-UVS instrument. This microchannel plate detector consists of a z-stack of three microchannel plates that amplify photoelectrons by a ~10^7 gain factor onto a cross-delay line (XDL) anode. These microchannel plates contain 12 μm pores with a length-to-diameter ratio of 80:1, for a total stack thickness of 2.9 mm. The anode is then read by a set of custom detector electronics that live a few inches behind the detector. The active area of the detector is approximately 38 mm by 18 mm. This Juno-UVS flight spare is identical in fit, form, and function to the detector assembly that will reach Jupiter aboard the Juno spacecraft in July 2016. This detector is driven by a ± 7.3V local power supply, with approximately -4kV from a high voltage supply necessary to drive the MCPs. The detector electronics output is read to a custom GSE unit via a 20+ meter-long cable from the experiment room in the basement, through shielded cable vias, to the control room on the first floor. Likewise, the HVPS lives in the control room so the operator may quickly shut down HV to the detector if necessary, with a 20+ meter HV cable between the HVPS and the detector. A relatively high (< 5×10^{-6} Torr) vacuum was maintained on the detector via a fore line connecting the detector manifold to the vacuum chamber containing the Van de Graaff generator. Local detector pressure was further reduced by a 2 L/s ion pump on the detector manifold. The detector is shown in its test position directly behind the Faraday cup in Figure 2.

The front of the detector contains a 3-mm thick fused silica window. This window fluoresced during the initial testing in July 2012, rendering the results difficult to analyze. The fluorescence was mitigated during the November 2013 tests by attaching a thin layer of UHV-compatible foil to the inside of the window. This foil blocked any UV emission due to fluorescence while allowing electrons to pass unimpeded. Pre-ship tests proved both the efficiency of the light block and the ability of the detector to operate nominally with the foil on the window.

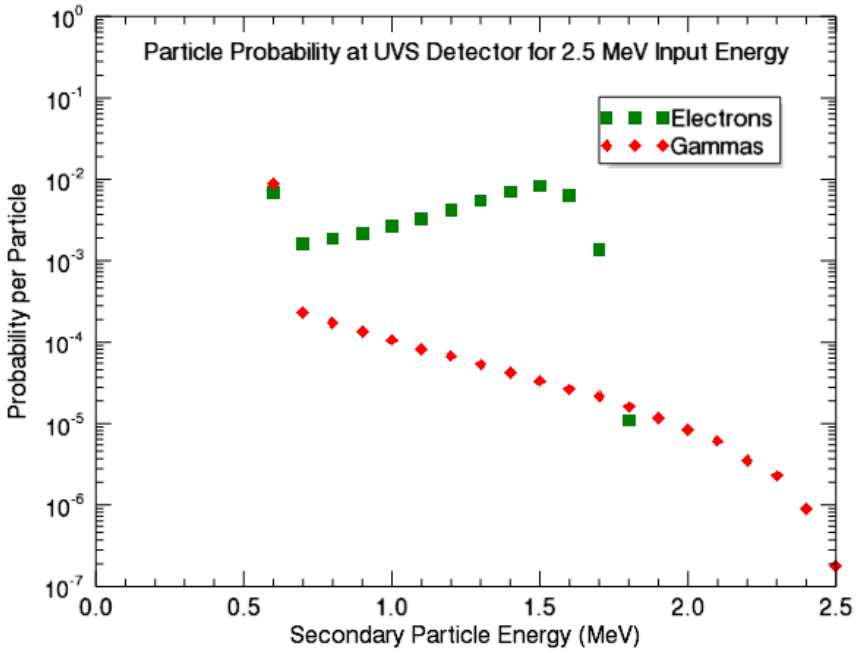

Figure 3. Probability per particle that a secondary particle reaching the Juno-UVS spare detector will have a certain energy for a primary electron with input energy of 2.5 MeV.

3. ELECTRON INTERACTION SIMULATIONS

While the fused silica window on the Juno-UVS spare detector transmits high-energy electrons, the passage of those electrons will create secondary gamma-rays and x-rays due to Bremsstrahlung. These secondaries must be modeled to understand the actual detector input, as there is no way to place a Faraday cup or similar detector within the existing Juno-UVS spare detector housing. MCNP6, full release version 1.0 of the Monte-Carlo N-Particle transport computer code, was employed to simulate the energy and flux loss along the beam centerline due to the Al exit window, the air gap, and the fused silica window on the Juno-UVS spare detector housing[6]. Results of MCNP6 simulations for four initial beam energies are shown in Figures 3-6. For each initial electron energy the fraction of initial beam intensity is presented after passing through the fused silica window near the MCP detector. Figure 3 shows the energy distribution of arriving electrons and photons in 100 keV bins for an initial energy of 2.5 MeV, with all energies below 0.6 MeV collected into a single bin. Note that the highest probability in the electron energy distribution is 1.5 MeV, with no electrons having energy above 1.8 MeV due to losses while penetrating the fused silica window. Figure 4 is the same as Figure 3 but for electrons with an initial energy of 2.0 MeV, and energy bins down to 100 keV. The energy distribution probability peaks at ~0.95 MeV, with no electrons having energy above 1.4 MeV due to penetration losses. Figure 5 shows the energy distribution for electrons with an initial energy of 1.5 MeV. The highest probability in the energy distribution is ~0.85 MeV, with no electrons having energy above 1.3 MeV. Note that in all three cases the photon energy is continuous all the way up to the input energy, indicating a small percentage of high energy electrons are stopped completely and converted to secondary gammas. However, the number of these secondary gammas is orders of magnitude lower than the electrons, so for energies of 2 MeV and above the secondaries can be ignored. For input energies of 1.5 MeV, the number of low energy photons approaches the number of higher energy electrons, so depending on the QE to "low" energy gamma photons, there could be confusion with electrons. Finally, Figure 6 shows the energy distribution for electrons with an initial energy of 0.5 MeV. In this case, electrons are almost entirely stopped by the fused silica windows and converted to secondary gammas and x-rays.

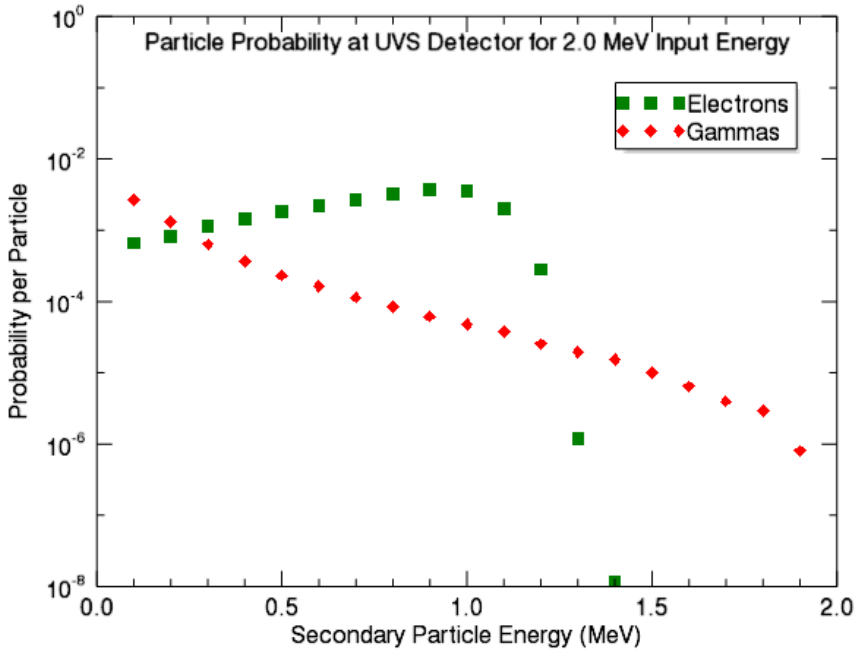

Figure 4. Probability per particle that a secondary particle reaching the Juno-UVS spare detector will have a certain energy for a primary electron with input energy of 2.0 MeV.

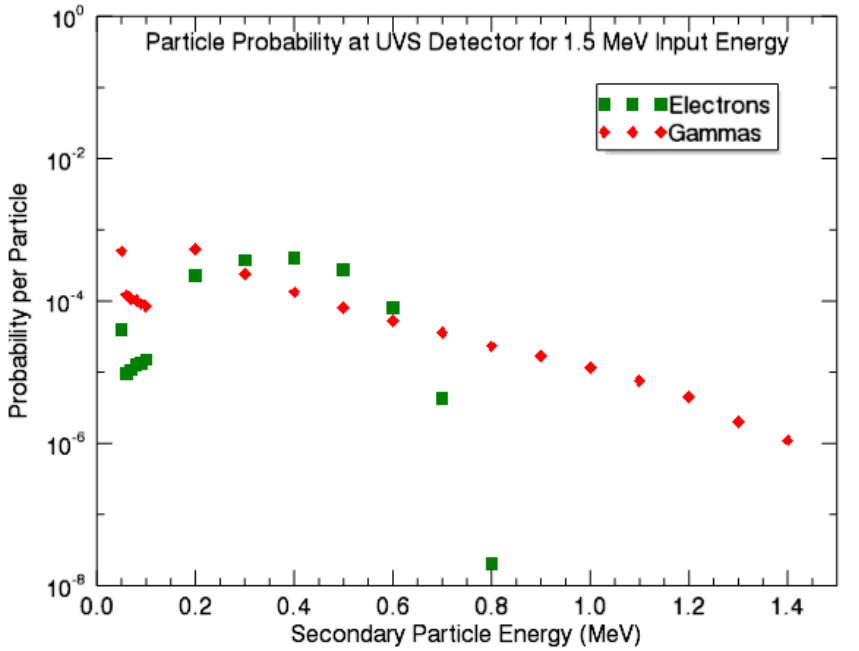

Figure 5 Probability per particle that a secondary particle reaching the Juno-UVS spare detector will have a certain energy for a primary electron with input energy of 1.5 MeV.

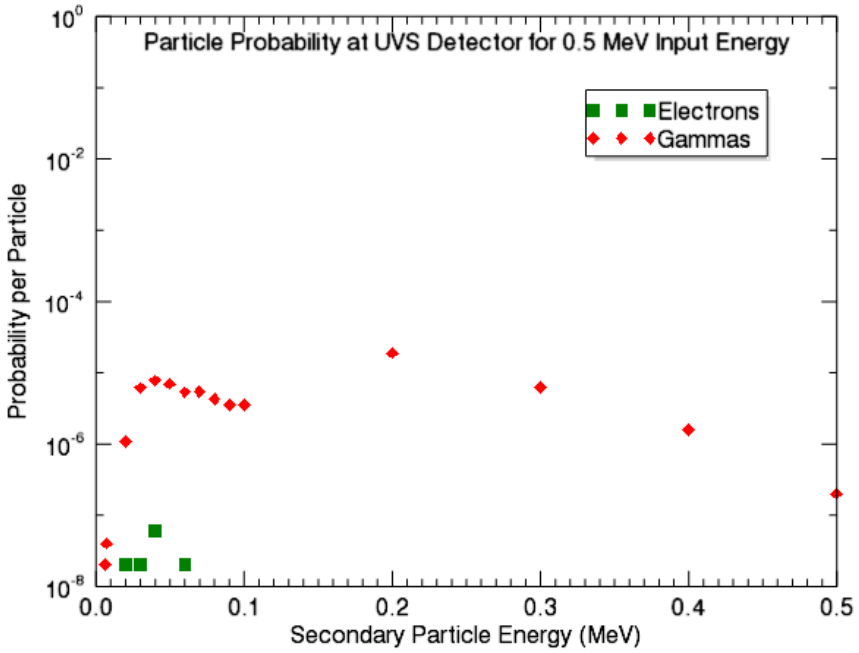

Figure 6. Probability per particle that a secondary particle reaching the Juno-UVS spare detector will have a certain energy for a primary electron with input energy of 0.5 MeV.

4. RESULTS

The Juno-UVS flight spare detector made measurements at four different input energies. As input energy increased, the beam current had to be reduced to avoid saturating the detector. The lower currents also tended to be unstable over time, so short exposures were taken with Faraday cup measurements before and after the exposures to verify beam current stability. Figure 7 shows the results of measurements at 2.3 (top), 1.9 (middle), and 1.5 (bottom) MeV. The blue area represents the active area of the detector. The white rectangle around the blue area is a box drawn in order to select the counting area. The white dots to the left and right of the active area are "stimulation pixels" created by the detector electronics. These stim pixels are a constant signal with known rate and location, and serve to ensure the detector electronics processing is working correctly. Finally, the area within the black rectangle represents the histogram image returned by the detector electronics. Energies above 2.3 MeV produced too many counts on the detector at stable output currents, so the maximum energy was capped at that level. The intermediate energy was then dropped from 2.0 MeV to 1.9 MeV to even the energy spacing between the three measurements. The 2.3 MeV beam produced a count rate of approximately 49 kHz on the detector with an input current of 250 fA. The 1.9 MeV beam produced a count rate of approximately 73 kHz on the detector with an input current of 750 fA. The 1.5 MeV beam produced a count rate of approximately 1800 Hz on the detector with an input current of 150 fA.

The images in Figure 7 show a slight intensity gradient from left-to-right, but not definitive "spot" from the input electron beam. This absence is probably due to the scattering and absorption effects of the fused silica window causing the overall beam to expand beyond the active area of the detector. Figure 8 shows the image on the flight spare detector with input beam energy of 0.5 MeV. At this low energy, the count rate was approximately 16 kHz on the detector with an input current of 85 pA.

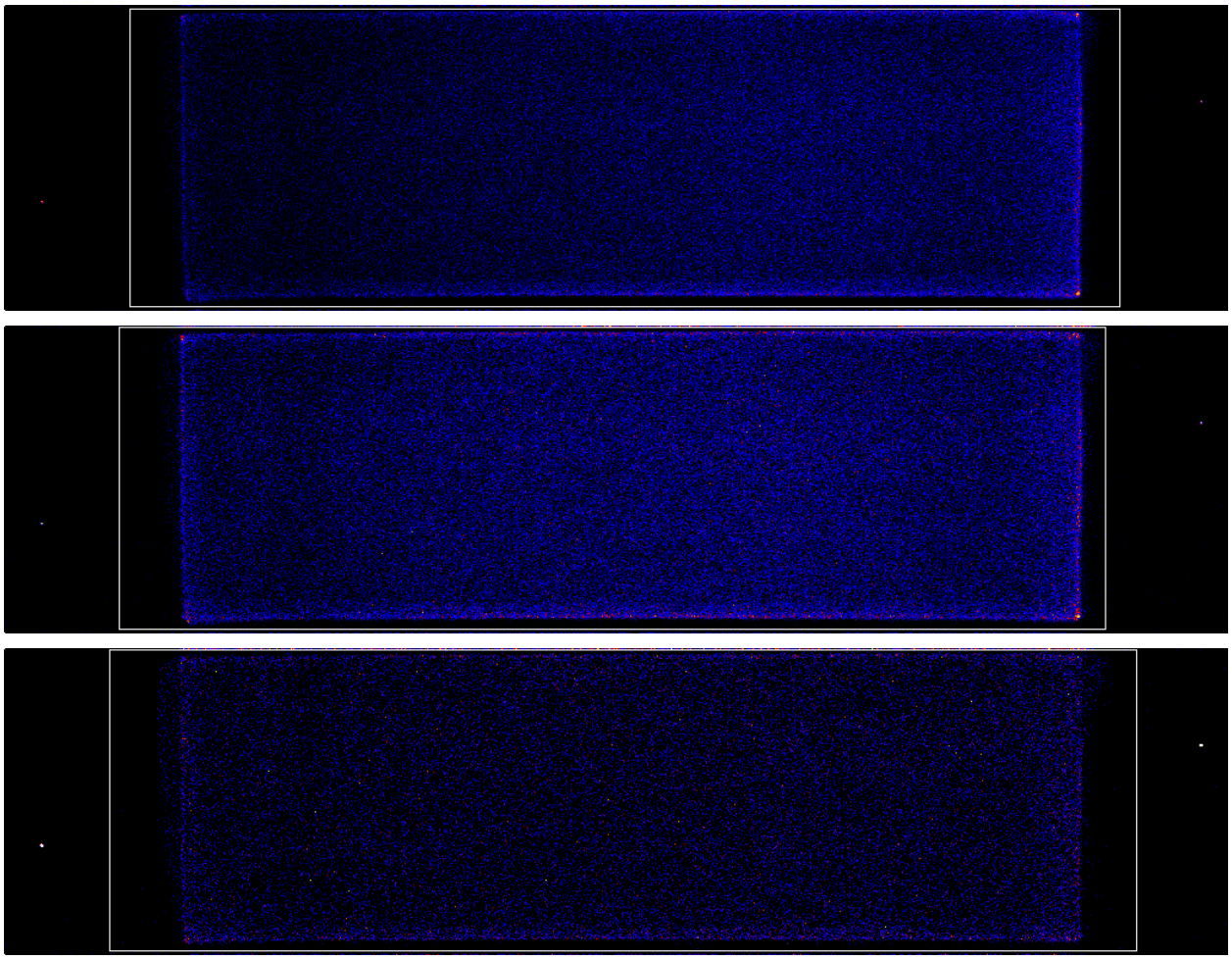

Figure 7. Juno-UVS spare detector images of electron beams with input energies of 2.3 MeV (top), 1.9 MeV (middle), and 1.5 MeV.

The results of the electron simulation are combined with the measured counts on the detector to determine the detector efficiency to electrons (for input energies of 1.5 MeV and greater) and gammas (for 0.5 MeV input energy). For each energy the sum of probabilities over each energy bin was multiplied by the input current to calculate the number of particles that actually reach the detector. For the 1.9 MeV and 2.3 MeV input energies these particles are assumed to be all electrons, while at 0.5 MeV they are assumed to be photons. For 1.5 MeV input energy it is assumed that enough of each particle reaches the detector that a "mix" must be determined. In that case, the detector QE to high energy photons from the 0.5 MeV measurement is used to calculate the photon number, and the remaining counts are assumed to be due to electrons. The uncertainties in these calculations are due to shot noise statistics on the flight spare detector, the stability of the input beam as measured by the Faraday cup before and after each run, and the number of digits shown in the current measurement. In other words, for a current measurement of 0.15 pA, the second digit is the last one shown on the meter, so the uncertainty is assumed to be 0.01 pA. These errors were summed in quadrature to determine the final uncertainty in the measurements.

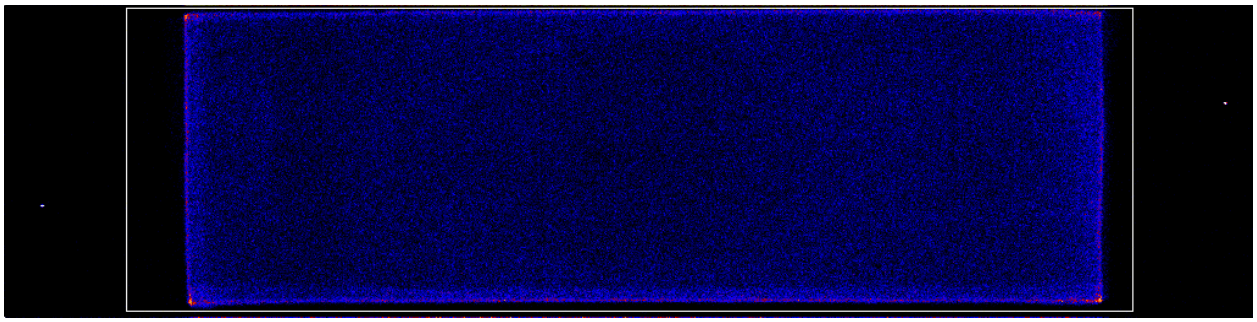

Figure 8. Juno-UVS spare detector image of electron beam with input energy of 0.5 MeV. Virtually all of the input electrons have been converted to secondary gamma-ray photons by the fused silica window in this case.

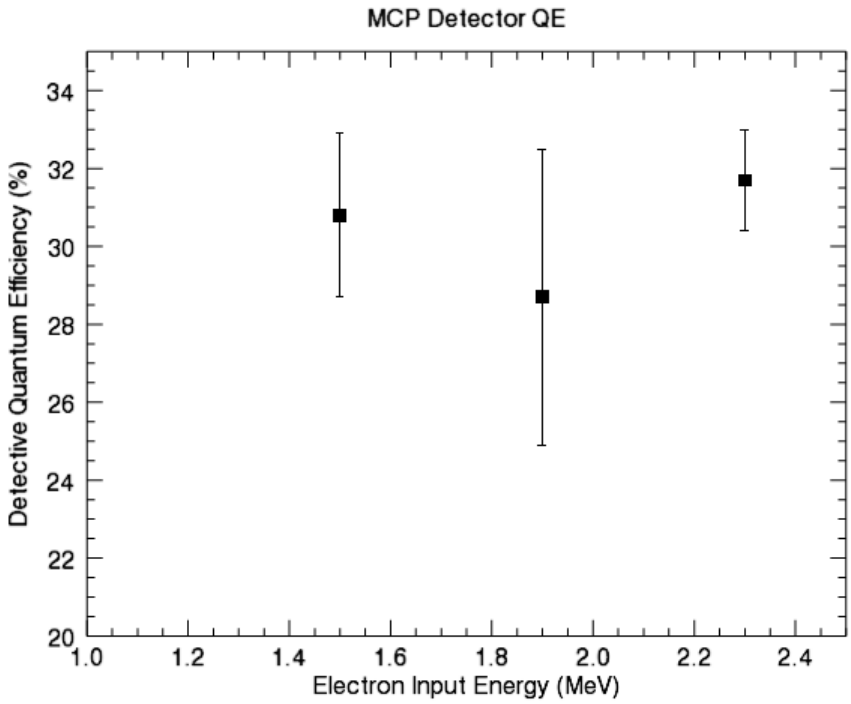

Figure 9. Juno flight spare detector efficiency to electrons as a function of beam input energy.

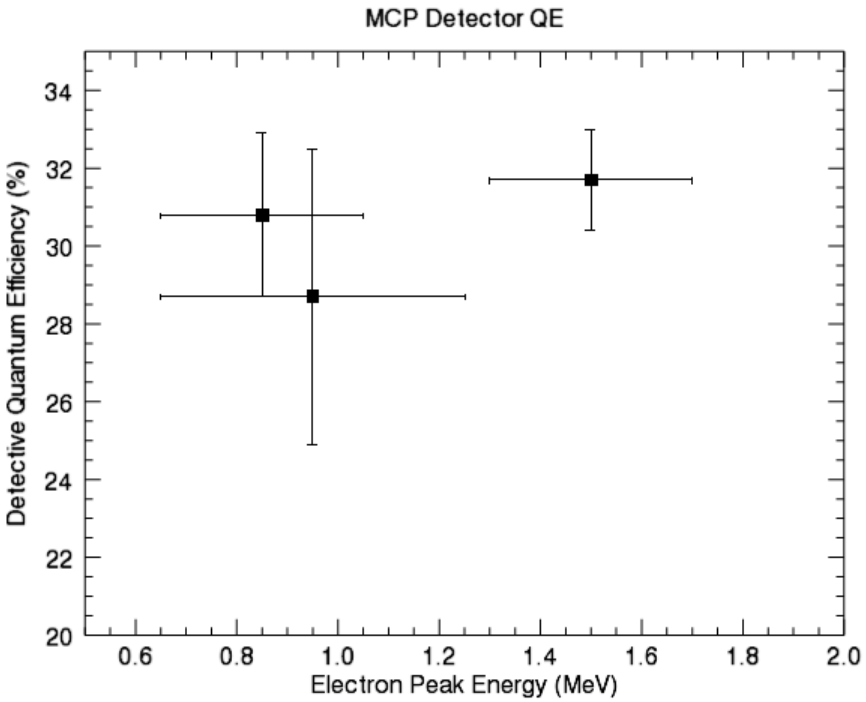

Figure 10. Juno flight spare detector efficiency to electrons as a function of electron peak energy at the detector as established by MCNP6 modeling.

The quantum efficiencies measured in this experiment agree with previous measurements made with similar detectors. The electron efficiency is shown in Figure 9 as a function of input energy, and in Figure 10 as a function of peak energy expected at the detector. The measured QE is 31±2% at 1.5 MeV input energy, 29±4% at 1.9 MeV input energy, and 32±1% at 2.3 MeV input energy. All three measurements are consistent with each other within the limits of experimental error, and consistent with the 33% QE measured by Pluto-Alice during New Horizon's Jupiter flyby[5]. These measurements are not consistent with the 4% to 15% efficiencies as a function of input energy ranging from 0.5 to 2.6 MeV measured by Blase *et al*[7]. However, that experiment consisted of a chevron MCP stack with much smaller pores and a total glass thickness of 150 μm, nearly 20 times thinner than the Juno-UVS spare detector MCP stack, so the different efficiencies in these and other higher-energy tests of similar devices planned for JUICE[8,9] are to be expected. Finally, the measured QE to gamma rays is 2.4±0.1% at 0.5 MeV input energy based on the electron-to-gamma conversion of the fused silica window. This measurement is consistent with the 2% QE to gammas reported by Siegmund *et al*[10].

5. CONCLUSION

The measured efficiency of the UVS-style microchannel plate detectors to MeV-level electrons is approximately 31%, consistent with previous measurements with UVS-style detectors, but not consistent with measurements by other microchannel plate detectors with thinner MCP stacks. The measured efficiency of UVS-style detectors to gamma rays is 2.4%, also consistent with previous measurements. Future refinements to these values may be achieved by creating a large vacuum chamber that can attach to the Van de Graff chamber output in order to operate a UVS-style detector with the door open. With the detector door open and the overall detector system in vacuum, there will be nothing in between the detector and the beam to create secondaries and/or a wide spectrum of electrons. Another improvement would be to run measurements with a cross-strip (XS) microchannel plate detector that is capable of running at 10x higher count rates than the Juno-UVS flight spare detector[11]. These detectors would allow the Van de Graaff generator to run at higher currents, which are inherently more stable than the low currents necessary for the Juno-UVS flight spare tests.

ACKNOWLEDGEMENTS

We wish to thank Greg Winters for experimental setup advice and insight, Oswald Siegmund and the group at Sensor Sciences for detector advice, and Jim Foster for building the long (20+ meters) cables necessary to connect the detector to the control room at the HVRL. This work was supported by SwRI internal research contract 15-R8324, by JPL contract #1340158, and NASA contract #NNN12AA01C.

REFERENCES

[1] Stern, S.A., Slater, D.C., Scherrer, J., Stone, J., Versteeg, M., A'Hearn, M.F., Bertaux, J.L., Feldman, P.D., Festou, M.C., Parker, J.Wm., and Siegmund, O.H.W., "Alice: The Rosetta Ultraviolet Imaging Spectrograph." Space Science Reviews 128, pp. 507-527 (2007).

[2] Stern, S.A., D.C. Slater, J.R. Scherrer, J.M. Stone, G.J. Dirks, M.H. Versteeg, M.W. Davis, G.R. Gladstone, J.Wm. Parker, L.A. Young, O.H.W. Siegmund Alice, "The ultraviolet imaging spectrograph aboard the New Horizons Pluto-Kuiper Belt mission." Space Science Reviews 140, 155–187 (2008).

[3] Gladstone, G. R., Stern, S. A., Retherford, K. D., Black, R. K., Slater, D. C., Davis, M. W.., Versteeg, M. H., Persson, K. B., Parker, J. W., Kaufmann, D. E., Egan, A. F., Greathouse, T. K., Feldman, P. D., Hurley, D., Pryor, W. R., and Hendrix, A. R., "*LAMP*: the Lyman Alpha Mapping Project on NASA's Lunar Reconnaissance Orbiter Mission," Space Science Reviews 150, pp. 161-181 (2010).

[4] Gladstone, G.R., Persyn, S.C., Eterno, J.S., Walther, B.C., Slater, D.C., Davis, M.W., Versteeg, M.H., Persson, K.B., Young, M.K., Dirks, G.J., Sawka, A.O., Tumlinson, J., Sykes, H., Beshears, J., Rhoad, C.L., Cravens, J.P., Winters, G.S., Klar, R.A., Lockhart, W. Piepgrass, B.M., Greathouse, T.K., Trantham, B.J., Wilcox, P.M., Jackson, M.W., Siegmund, O.H.W., Vallerga, J.V., Raffanti, R., Martin, A., Gerard, J.-C., Grodent, D.C., Bonfond, B., Marquet, B., and Denis, F., "The Ultraviolet Spectrograph on NASA's Juno Mission," Space Science Reviews, doi: 10.1007/s11214-014-0040-z (2014).

[5] Steffl, A.J., A.B. Shinn, G.R. Gladstone, J.W. Parker, K.D. Retherford, D.C. Slater, M.H. Versteeg, and S.A. Stern (2012), "MeV electrons detected by the Alice UV spectrograph during the *New Horizons* flyby of Jupiter", *Journal of Geophysical Research, 117*, A10222, doi:10.1029/2012JA017869.

[6] Gorely, J.T. *et al.*, MCNP6 User's Manual Version 1.0 May 2013.

[7] Blase, R.C., R.R. Benke, C.M. Cooke, and K.S. Pickens, "Microchannel Plate Detector Detection Efficiency to Monoenergetic Electrons Between 0.4 and 2.6 MeV", *IEEE Transactions on Nuclear Science*, 62, 6, pp. 3339-3345 (2015)

[8] Tulej, M., S. Meyer, M. Luthi, D. Lasi, A. Galli, L. Desorgher, W. Hajdas, S. Karlsson, L. Kalla, P. Wurz, "Detection efficiency of microchannel plates for e(-) and pi(-) in the momentum range from 17.5 to 345 MeV/c", *Rev Sci Instrum*, 86 (2015).

[9] MacDonald, E.A., M.F. Thomsen, H.O. Funsten, "Background in channel electron multiplier detectors due to penetrating radiation in space", *IEEE T Nucl Sci*, 53 (2006) 1593-1598.

[10] Siegmund, O.H.W., C. Ertley, and J. Vallerga, "High Speed Large Format Photon Counting Microchannel Plate Imaging Sensors", *Proceedings of the Advanced Maui Optical and Space Surveillance Technologies Conference*, held in Wailea, Maui, Hawaii, September 15-18, 2014, Ed.: S. Ryan, The Maui Economic Development Board, id.94 (2015)

[11] Vallerga, J., R. Raffanti, M. Cooney, H. Cumming, G. Varner, and A. Seljak, "Cross strip anode readouts for large format, photon counting microchannel plate detectors: developing flight qualified prototypes of the detector and electronics", Proceedings of the SPIE, Volume 9144, id. 91443J (2014)